Role of projectile electrons for target-recoil-charge-state production in intermediate-energy B^{2+}-Ne collisions

Gerald Schenk,* Marko Horbatsch, and Tom Kirchner
Department of Physics and Astronomy, York University, Toronto, Ontario, Canada M3J 1P3
(Received 31 May 2013; published 24 July 2013)

We apply an independent electron model to study q-fold target-charge-state production in 25–600 keV/nucleon B^{2+}-Ne collisions for which experimental and theoretical results were published recently [W. Wolff *et al.*,Phys. Rev. A **84**, 042704 (2011)]. The model treats projectile and target electrons using a common potential and makes use of a single-determinant wave function for the combined system. The calculated total cross sections for positive recoil ion production as well as for Ne^{q+} production ($q = 1, \ldots, 4$) determined in coincidence with an unchanged projectile charge state agree well with experiment where available, i.e., in the 30–400 keV/nucleon energy range. At energies below 200 keV/nucleon the projectile electrons are shown to play a crucial role in reproducing the experimental data for $q = 1, \ldots, 4$. For the $q \geqslant 2$ channels the inclusion of projectile electron contributions is needed even at energies above 200 keV/nucleon in order to reproduce the experimental data. As expected, the predictions for the $q = 5$ recoil charge state overestimate the experimental data due to a failure of the independent electron model for this extreme channel.

DOI: 10.1103/PhysRevA.88.012712 PACS number(s): 34.50.Fa, 34.70.+e

I. INTRODUCTION

Collisions of atoms with ions which carry electrons are common in nature and have become the subject of detailed experimental investigation [1–10]. Quantities that were studied include total recoil-charge-state production [2,3], free-electron production [2], q-fold recoil production [4], charge-state correlated cross sections [5–9], as well as projectile-angle differential cross sections [10]. For fast, distant collisions one might expect these collisions to be very similar to bare-ion impact with the correct effective charge. For close collisions (both fast and slow) this assumption needs to be looked at. Collisions with active projectile electrons are, however, difficult to describe theoretically, in particular at intermediate energies (several keV/nucleon to 1 MeV/nucleon) where electron-transfer processes have to be considered.

An example of such a system is B^{2+}-Ne with three projectile electrons in the initial state. For this system Wolff *et al.* [11] measured total cross sections for target ionization processes coincident with unchanged projectile charge state in the energy range from 0.75 to 4 MeV ($m_{\text{boron}} = 11$ u). The same article also presents results from a (perturbative) continuum-distorted wave with eikonal initial state (CDW-EIS) [12,13] calculation. To deal with the dressed projectile an effective charge was defined based on the momentum transfer and found through the first-order Born approximation [14]. Based on an independent-particle-model (IPM) description the method yields single-particle ionization probabilities. Total cross sections for multiple-target ionization were obtained using multinomial combinatorics [11]. Other CDW-EIS calculations involving dressed projectiles were published in Refs. [15–18].

In this work, we address the B^{2+}-Ne collision system using the two-center basis generator method (TC-BGM) [19]. Our calculation is also based on an IPM, but it is nonperturbative and it allows the projectile electrons to participate actively and undergo transitions. Each active electron is subject to a mean-field potential representing the electron-electron interaction and the Coulomb potentials of both centers. Propagating the system for all independent initial conditions leads to the wave function of the combined system on the level of a single determinant.

Transition probabilities for specific collision channels are calculated by projecting this wave function onto final states, which are also represented by single determinants [20,21]. At the level of this final-state analysis we have a choice to consider both target and projectile electrons or to neglect the latter, i.e., to consider the target electrons only. Comparing the results of both analyses with each other and with the experimental data sheds light on the role the projectile electrons play in the collision. In contrast with an IPM based on multinomial statistics the present work deals explicitly with Pauli correlations.

Atomic units ($\hbar = m_e = e = 4\pi\epsilon_0 = 1$) are used throughout the article, unless stated otherwise.

II. METHOD

The collision problem is treated by the semiclassical impact-parameter approximation using a straight-line trajectory for the motion of the nuclei. The electronic system is treated quantum mechanically within the single-determinant IPM. The electron-electron interaction is incorporated through the mean field of the electrons. It gives rise to effective potentials v_{ee}^{t} and v_{ee}^{p} in the Hamiltonian

$$\hat{h}(t) = -\frac{1}{2}\Delta - \frac{Z_{\text{t}}}{r_{\text{t}}} - \frac{Z_{\text{p}}}{r_{\text{p}}} + v_{ee}^{\text{t}}(r_{\text{t}}) + v_{ee}^{\text{p}}(r_{\text{p}}). \qquad (1)$$

Here Z_{t} and Z_{p} are the charge numbers of the target and projectile nuclei, respectively. Since we work in the center-of-mass system, the distances of the active electron to the target nucleus r_{t} and to the projectile nucleus r_{p} both depend on time.

*gschenk@yorku.ca

The effective target potential v_{ee}^{t} consists of a Hartree term and an exchange term. The Hartree potential represents the screening due to the charge density of all target electrons. The exchange term compensates for the self-interaction contained in the Hartree term. In our calculations we use an exchange potential resulting from the optimized potential method (OPM) [22]. For the effective projectile potential v_{ee}^{p} only the Hartree term is considered; i.e.,

$$v_{ee}^{\mathrm{p}}(r_{\mathrm{p}}) = \int \frac{2\left|\psi_{1s}^{\mathrm{B}^{2+}}(r)\right|^2 + \left|\psi_{2s}^{\mathrm{B}^{2+}}(r)\right|^2}{|\mathbf{r}-\mathbf{r}_{\mathrm{p}}|} d^3r, \tag{2}$$

with (normalized) $1s$ and $2s$ orbitals obtained from an OPM calculation for $\mathrm{B}^{2+}(1s^2 2s)$ [22]. This choice of potentials results in the following asymptotic behavior: $-1/r_{\mathrm{t}}$ for the target, and $-2/r_{\mathrm{p}}$ for the projectile. This is correct for active *target* electrons before the collision. For an active *projectile* electron this potential choice may lead to an overestimation of processes removing population from projectile states. Such processes play only an indirect role in target ionization, namely through transfer ionization processes and projectile-charge-state coincident channels. A more detailed discussion of this matter can be found in Refs. [23,24].

With the Hamiltonian (1) the system can be propagated using a set of single-particle equations

$$i\,\partial_t \psi_i(\boldsymbol{r},t) = \hat{h}(t)\psi_i(\boldsymbol{r},t), \quad i = 1,\ldots,K, \tag{3}$$

each corresponding to one of the initial conditions. We solve these equations using a finite basis expansion. The basis consists of atomic neon eigenstates ($2s$ to $4f$), the $1s$ to $4f$ eigenstates of the projectile Hamiltonian $-\frac{1}{2}\Delta - \frac{Z_{\mathrm{p}}}{r_{\mathrm{p}}} + v_{ee}^{\mathrm{p}}(r_{\mathrm{p}})$, and pseudostates generated with the TC-BGM [19] from target states. Not included in the basis is the target $1s$ state, as its role is insignificant [11]. The pseudostates are generated from the target states by applying powers ν of a regularized projectile potential operator. A total of 126 pseudostates are included, up to a maximum hierarchy level of $\nu = 6$, to ensure convergence with respect to basis size.

Using the same Hamiltonian and the same basis for all active electrons ensures that the propagated orbitals remain orthogonal throughout the collision and can be combined at the final time to form a single Slater determinant. When this determinant is projected onto many-electron states which are also represented by single Slater determinants, exclusive transition probabilities to these final configurations are obtained as a function of impact parameter b. Note that the antisymmetry property of Slater determinants ensures that the Pauli principle is respected.

Typically, a large number of final configurations contribute to an experimentally accessible collision channel, e.g., to one of the charge-state coincidences measured by Wolff *et al.* [11]. In such cases the inclusive-probabilities scheme [20] provides a way to calculate the desired probabilities without carrying out the large summations over all contributing final configurations explicitly. Its key idea is the insight that one can express the inclusive probability to find q out of N electrons in a fully specified subconfiguration, while the remaining $N-q$ electrons are not observed, as a $q \times q$ determinant of the one-particle density matrix. Probabilities that correspond to charge-state coincidences can then be calculated as (ordered) sums over these inclusive probabilities, which reduces the computational cost tremendously.

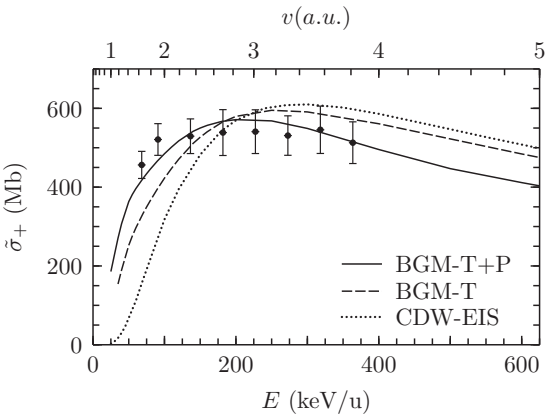

FIG. 1. Total cross section for positive ion production $\tilde{\sigma}_+$ as defined in Eq. (4) on the basis of the $q = 1,\ldots,5$ cross sections $\tilde{\sigma}_q$. The experimental data are from Table I of Wolff *et al.* [11] and are added according to Eq. (4). Present theory with final-state analysis that considers active target and projectile electrons (solid line), and target electrons only (dashed line). Target-only CDW-EIS [11] (dotted line).

This determinant analysis for a single-center BGM calculation using a coupled mean-field approach to address the projectile electrons is described in Ref. [7]. Its application to analyzing a TC-BGM calculation is described in Ref. [25]. We perform the analysis considering all target electrons, except those of the K shell, and all projectile electrons, namely by solving Eq. (3) for the $1,\ldots,K$ initial conditions: Ne ($2s\uparrow\downarrow$, $2p_0\uparrow\downarrow$, $2p_{-1}\uparrow\downarrow$, $2p_{+1}\uparrow\downarrow$), B^{2+} ($1s\uparrow\downarrow$, $2s\uparrow$). The results of this 11-electron calculation are referred to as BGM-T + P.

For comparison purposes a final-state analysis considering the eight target electrons only is also performed and labeled as BGM-T in the following. The latter calculation is based on the same TC-BGM calculation, but it ignores transition amplitudes from projectile initial conditions. From an IPM perspective it is thus similar in spirit to the statistical analysis of the CDW-EIS calculation in Ref. [11], except that it accounts for Pauli correlations within the target.

III. RESULTS

We begin the comparison of theoretical results and experiment with an inclusive channel of the collision in Fig. 1: the positive-ion-production cross section $\tilde{\sigma}_+$ from the neon target in coincidence with the final projectile charge state of B^{2+}, defined as a weighted sum

$$\tilde{\sigma}_+ = \sum_{q=1}^{5} q\tilde{\sigma}_q \tag{4}$$

of total cross sections

$$\tilde{\sigma}_q = 2\pi \int_0^{b_{\max}} \tilde{P}_q(b) b\, db \tag{5}$$

for q-fold recoil ion production $\mathrm{B}^{2+} + \mathrm{Ne}^0 \rightarrow \mathrm{B}^{2+} + \mathrm{Ne}^{q+}$. In Eq. (5) we chose $b_{\max} = 12$ a.u. The sum in Eq. (4) is truncated at the highest available experimental value of q.

Note that this channel is inclusive in the recoil charge, but is projectile-charge-state specific.

The total cross section $\tilde{\sigma}_+$ is shown as a function of the projectile kinetic energy per nucleon (bottom axis), while the top axis provides as a reference the relative velocity in atomic units. Above 200 keV/nucleon the BGM-T model results (dashed line) are in good agreement with those from the CDW-EIS model (dotted line). Both are slightly higher than experiment. The BGM-T results deviate from the CDW-EIS calculations at energies below 200 keV/nucleon. A possible cause for the discrepancy might be limitations of the (perturbative) CDW-EIS model, which is not expected to be valid below 100 keV/nucleon due to its limitations in representing single-electron dynamics in a two-center situation with the possibility of electron transfer. However, at 100 keV/nucleon and below, the BGM-T calculations also disagree substantially with the experiment.

The present calculation which takes target and projectile electrons into account in the final-state analysis, BGM-T + P (solid line), does a better job at low energies. It is also more consistent with experiment over the entire energy range. The slight underestimation of the two lowest-energy experimental data points raises the question whether an improved dynamical calculation using time-dependent response [26] would yield better agreement.

A look at the total cross sections $\tilde{\sigma}_q$ for q-fold recoil ion production provides a more detailed picture, shown in Fig. 2 for $q = 1, \ldots, 5$. The BGM-T + P results for single ionization ($q = 1$) fall short of the experiment at the lowest energies, which is also reflected in the $\tilde{\sigma}_+$ results discussed above. For $q = 2$ and $q = 3$, however, such a shortfall at low energies does not appear: while the BGM-T model fails to describe the collisions at low energies, BGM-T + P is in good agreement with the experiment for all energies. At about 200 keV/nucleon the BGM curves intersect, and the BGM-T + P results are above the BGM-T data at low energies, and below at high energies. An explanation for the latter can be found in the nonzero probability for direct projectile electron loss at high energies. At low energies the indistinguishable nature of electrons, which is accommodated in our Slater determinant description, allows for the increase compared to the BGM-T calculation and results in closer agreement with the experimental data.

More concretely, we find that a transfer ionization process, in which capture of a target electron by the projectile is accompanied by projectile electron loss to the continuum, contributes significantly to q-fold recoil ion production without change of the B^{2+} charge state in this region. In principle, we have to be careful with such contributions, since the single-particle potential employed has asymptotic properties for projectile electrons which make their removal possibly too easy. This was noted recently in the context of He^+ collisions with water molecules [23,24]. For the present case, however, we find that the BGM-T + P calculations follow the experimental data better than the pure target calculations. This lends support to the notion that—at least in the case of the present collision system—projectile electron removal does indeed contribute significantly to the channel presented. A physical reason for the difference between the two collision systems with projectile electrons is that the present B^{2+}-Ne system is less asymmetric in electron occupation number on projectile and target.

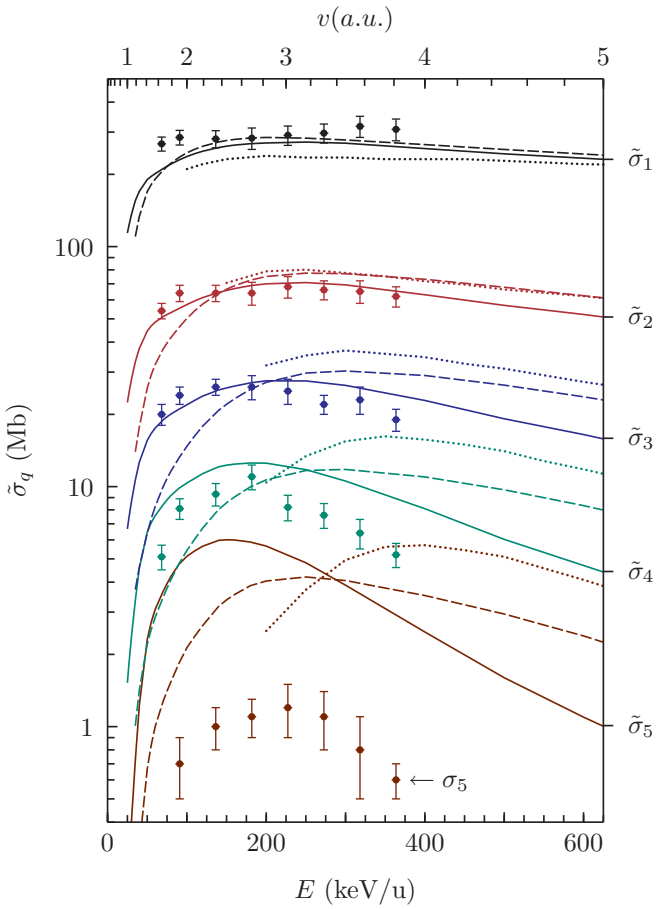

FIG. 2. (Color online) Total cross sections $\tilde{\sigma}_q$ for q-fold recoil ion production coincident with (unchanged) projectile charge state: $B^{2+} + Ne^0 \rightarrow B^{2+} + Ne^{q+}$ as functions of projectile energy. The experimental data are from Wolff *et al.* [11]. Present theory with final-state analysis that considers active target and projectile electrons (BGM-T + P) (solid line), and target electrons only (BGM-T) (dashed line). Target-only CDW-EIS [11] (dotted line).

There is a known limitation of IPM calculations describing multiple-target ionization: they typically work well as long as the final target charge state does not exceed that of the projectile by much more than 1. This limitation of the IPM was found in previous work for He^{2+}-Ne [26], p-Ar and He^{2+}-Ar [27], C^{4+}-Ne [28], and more recently in p-H_2O collision calculations [29]. It is also reflected in the present results. For $q = 3$ the agreement of the BGM-T + P calculation with the experimental data is very good. For $q = 4$ the experiment is somewhat overestimated, but the BGM-T + P curve resembles the overall structure of the experimental points rather well. For $q = 5$ the calculation overestimates the measurements by about a factor of 5 and differs in shape.

In Fig. 3 we return to an inclusive quantity, which is related to the total recoil ion production shown in Fig. 1. The average charge

$$\langle q \rangle = \frac{\sum_{q=1}^{q_{\max}} q\tilde{\sigma}_q}{\sum_{q=1}^{q_{\max}} \tilde{\sigma}_q} = 1 + \frac{\sum_{q=1}^{q_{\max}} (q-1)\tilde{\sigma}_q}{\sum_{q=1}^{q_{\max}} \tilde{\sigma}_q} \qquad (6)$$

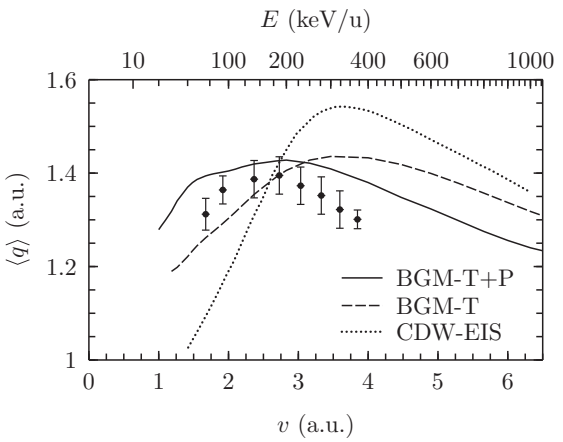

FIG. 3. Average recoil ion charge $\langle q \rangle$ as defined in Eq. (6) on the basis of the $q = 1, \ldots, 4$ cross sections $\tilde{\sigma}_q$. Experimental data from Wolff *et al.* [11]. Present theory with final-state analysis that considers active target and projectile electrons (solid line), and target electrons only (dashed line). Target-only CDW-EIS [11] (dotted line).

is defined by dividing this total cross section by the sum of individual recoil-ion-production cross sections to remove some uncertainty associated with absolute cross-section determinations. The sums are truncated at $q_{\max} = 4$ as in Ref. [11]. Equation (6) does represent an average charge state obtained in ionizing collisions, while averaging over impact parameters: high-charge-state probabilities occur for small b, then $q = 1$ dominates for large b.

It is interesting to observe that this quantity emphasizes the differences between the models. The inclusion of active projectile electrons (BGM-T + P) leads to an increased recoil charge for $v \lesssim 2$ a.u., since projectile electron loss makes room for enhanced transfer of electrons from the target. For $v \gtrsim 3$ a.u., on the other hand, the inclusion of active projectile electrons results in a reduction of the recoil charge state. From Fig. 2 we conclude that this is primarily due to loss of projectile electrons affecting predominantly high-target-charge states. Such loss processes occur in close collisions ($b < 1$ a.u.), where multiple-target ionization also happens. In contrast, single-target-ionization probabilities are high for a much wider range of impact parameters.

IV. CONCLUSIONS

Full two-center IPM calculations for the B^{2+}-Ne collision system were carried out using the basis generator method. They were analyzed within an inclusive single-determinant framework using two points of view: with and without the inclusion of active projectile electron participation, labeled as BGM-T + P and BGM-T, respectively. The comparison with experimental data reveals that charge-exchange processes and projectile electron loss to the continuum play a significant role at collision energies below 100 keV/nucleon, and are also noticeable at high energies. The latter is particularly true for recoil charge-state production to $q = 3,4$ (in coincidence with $B^{2+} \rightarrow B^{2+}$). It is remarkable that the inclusive results shown in Figs. 1 and 3 are also strongly affected.

ACKNOWLEDGMENTS

The financial support of NSERC Canada is gratefully acknowledged. We thank Mitsuko Murakami for helpful discussions.

[1] C. Cocke and R. Olson, Phys. Rep. **205**, 153 (1991).
[2] M. E. Rudd, T. V. Goffe, A. Itoh, and R. D. DuBois, Phys. Rev. A **32**, 829 (1985).
[3] S. H. Be, T. Tonuma, H. Kumagai, H. Shibata, H. Kase, T. Kambara, I. Kohno, and H. Tawara, J. Phys. B **19**, 1771 (1986).
[4] C. L. Cocke, Phys. Rev. A **20**, 749 (1979).
[5] T. J. Gray, C. L. Cocke, and E. Justiniano, Phys. Rev. A **22**, 849 (1980).
[6] T. Tonuma, H. Kumagai, T. Matsuo, and H. Tawara, Phys. Rev. A **40**, 6238 (1989).
[7] T. Kirchner, A. C. F. Santos, H. Luna, M. M. Sant'Anna, W. S. Melo, G. M. Sigaud, and E. C. Montenegro, Phys. Rev. A **72**, 012707 (2005).
[8] W. Wolff, H. Luna, A. C. F. Santos, E. C. Montenegro, and G. M. Sigaud, Phys. Rev. A **80**, 032703 (2009).
[9] J. S. Ihani, H. Luna, W. Wolff, and E. C. Montenegro, J. Phys. B **46**, 115208 (2013).
[10] S. Kelbch, C. L. Cocke, S. Hagmann, M. Horbatsch, C. Kelbch, R. Koch, H. Schmidt-Bocking, and J. Ullrich, J. Phys. B **23**, 1277 (1990).
[11] W. Wolff, H. Luna, A. C. F. Santos, E. C. Montenegro, R. D. DuBois, C. C. Montanari, and J. E. Miraglia, Phys. Rev. A **84**, 042704 (2011).
[12] D. S. F. Crothers and J. F. McCann, J. Phys. B **16**, 3229 (1983).
[13] P. D. Fainstein, V. H. Ponce, and R. D. Rivarola, J. Phys. B **21**, 287 (1988).
[14] J. E. Miraglia and M. S. Gravielle, Phys. Rev. A **81**, 042709 (2010).
[15] C. C. Montanari, E. C. Montenegro, and J. E. Miraglia, J. Phys. B **43**, 165201 (2010).
[16] C. C. Montanari, J. E. Miraglia, W. Wolff, H. Luna, A. C. F. Santos, and E. C. Montenegro, J. Phys: Conf. Ser. **388**, 012036 (2012).
[17] J. M. Monti, R. D. Rivarola, and P. D. Fainstein, J. Phys. B **41**, 201001 (2008).
[18] J. M. Monti, R. D. Rivarola, and P. D. Fainstein, J. Phys. B **44**, 195206 (2011).
[19] M. Zapukhlyak, T. Kirchner, H. J. Lüdde, S. Knoop, R. Morgenstern, and R. Hoekstra, J. Phys. B **38**, 2353 (2005).
[20] H. J. Lüdde and R. M. Dreizler, J. Phys. B **18**, 107 (1985).
[21] T. Kirchner and M. Horbatsch, Phys. Rev. A **63**, 062718 (2001).
[22] E. Engel and S. H. Vosko, Phys. Rev. A **47**, 2800 (1993).
[23] T. Kirchner, M. Murakami, M. Horbatsch, and H. J. Lüdde, J. Phys: Conf. Ser. **388**, 012038 (2012).

[24] M. Murakami, T. Kirchner, M. Horbatsch, and H. J. Lüdde, Phys. Rev. A **86**, 022719 (2012).
[25] M. Murakami, T. Kirchner, M. Horbatsch, and H. J. Lüdde, Phys. Rev. A **85**, 052704 (2012).
[26] T. Kirchner, M. Horbatsch, H. J. Lüdde, and R. M. Dreizler, Phys. Rev. A **62**, 042704 (2000).
[27] T. Kirchner, M. Horbatsch, and H. J. Lüdde, Phys. Rev. A **66**, 052719 (2002).
[28] T. Kirchner, M. Horbatsch, and H. J. Lüdde, Phys. Rev. A **64**, 012711 (2001).
[29] M. Murakami, T. Kirchner, M. Horbatsch, and H. J. Lüdde, Phys. Rev. A **85**, 052713 (2012).